

Article

Nonlinear Optical Properties of Zirconium Diselenide and Its Ultra-Fast Modulator Application

Mengxiao Wang ¹, Yue Zheng ¹, Linguang Guo ¹, Xiaohan Chen ², Huanian Zhang ^{3,*} and Dengwang Li ^{1,*}

¹ Shandong Province Key Laboratory of Medical Physics and Image Processing Technology, School of Physics and Electronics, Shandong Normal University, Jinan 250014, China; 2016020640@stu.sdnu.edu.cn (M.W.); yuezheng_9412@163.com (Y.Z.); linguang_guo@163.com (L.G.)

² School of Information Science and Engineering, and Shandong Provincial Key Laboratory of Laser Technology and Application, Shandong University, Jinan 250014, China; cxh@sdu.edu.cn

³ School of Physics and Optoelectronic Engineering, Shandong University of Technology, Zibo 255049, China

* Correspondence: zhn@sdnu.edu.cn (H.Z.); dengwang@sdnu.edu.cn (D.L.); Tel.: +86-531-86180521 (H.Z.); +86-531-86180216 (D.L.)

Received: 9 September 2019; Accepted: 1 October 2019; Published: 4 October 2019



Abstract: Recently, two-dimensional (2D) materials have been widely studied by researchers due to their exceptional 2D structure and excellent optical characteristics. As one of the typically-layered 2D transition metal dichalcogenide (TMD) semiconductors from group IVB with a bandgap value of 0.9–1.2 eV (bulk to monolayer), the characteristics of zirconium diselenide (ZrSe₂) have already been extensively investigated in many fields. However, the nonlinear absorption properties of ZrSe₂ in ultra-fast lasers have not been previously demonstrated. In this work, we measured various parameters in order to investigate the characteristics of the nonlinear saturable absorption of ZrSe₂. A ZrSe₂-polyvinyl alcohol (PVA) film was successfully prepared, which was employed as a saturable absorber (SA) to demonstrate, for the first time, an erbium (Er)-doped passive mode-locking fiber laser with a ring cavity. The saturation intensity of the ZrSe₂-PVA film-type SA is 12.72 MW/cm², while its modulation depth is 2.3%. The stable soliton state with a maximum output power of 11.37 mW and a narrowest monopulse duration of 12.5 ps at a repetition frequency of 21.22 MHz was detected. The experimental results conclusively proved that ZrSe₂, with its suitable bandgap value and excellent nonlinear absorption properties, as well as its high damage threshold, should have extensive potential applications within the field of ultra-fast pulse lasers.

Keywords: Zirconium diselenide (ZrSe₂); nonlinear absorption properties; saturable absorber (SA); Er-doped fiber laser; passively mode-locked fiber laser

1. Introduction

Mode-locked fiber lasers have been arousing the extensive interest of many researchers due to their value in a variety of applications in the fields of basic science, fiber telecommunications, industrial materials processing, precise optical metrology, biomedical imaging, and others [1–10]. Currently, there are normally two strategies, actively mode-locked and passively mode-locked technologies, that are employed to realize the mode-locked operation in a fiber laser. In order to achieve the actively mode-locked scheme, an acoustic-optic or electro-optic modulator is usually essential, which makes the laser complex so that it becomes difficult to achieve miniaturization. Compared to the actively mode-locked method, the passively mode-locked technique has more attractive advantages, such as no requirement for modulators, low cost, a compact structure, good stability, etc. Thus, it has been desired for a variety of studies and applications [9,11]. As is known, the nonlinear optical element, called a

saturable absorber (SA), is one of the key devices for achieving various ultra-short pulse trains and enhancing the stability of the environment in a passively mode-locking fiber laser [4,12]. Therefore, the study of novel and high performance SAs has always been the focus of ultrafast laser research.

Over the past decade, extensive investigations on various two-dimensional (2D) materials, which were employed as SAs because of their excellent nonlinear saturable absorption characteristics, have actually facilitated the rapid development of passively mode-locking fiber lasers [8]. As we all know, the discovery of graphene plays a crucial role in the exploration of novel 2D SAs [13–22]. Graphene exhibits excellent ultra-broadband absorption characteristics as a SA due to its unique bandgap structure [23–27]. However, two main disadvantages of graphene, the weak modulation depth of about 1.3% per layer and the difficulty in creating an optical bandgap, restricted its further in-depth application in passive mode-locking fiber lasers [4,28]. Since then, after graphene has been widely studied, different kinds of graphene-like 2D materials, including topological insulators (TIs) [29–36], transition metal dichalcogenides (TMDs) [37–41], and black phosphorus (BP) [42–47], have been widely used as SAs for investigating the characteristics of passively mode-locking fiber lasers. Significant progress has been made in the study of the SA base on these layer-structured 2D materials recently. Based on this, exploration of the new types of SAs with high damage thresholds, broadband absorption and ultrafast recovery time is still urgent due to the ever-increasing demand for mode-locked fiber lasers.

Recently, 2D semiconducting TMDs from group IVB, with the chemical formula MX_2 ($M = \text{Ti, Zr, Hf}$; $X = \text{S, Se, Te}$) have been extensively investigated because of their suitable wide-range bandgaps, their superior physical, electronic, magnetic, electrochemical, and photoelectrochemical (PEC) properties, and so on [48–53]. It has been reported that a stable TMD monolayer from group IVB is formed by one plane of a transition metal (M) and two slabs of chalcogen atoms (X), called a X-M-X-type sandwich, where M and X atoms are tightly bonded together by covalent bonding, and the layers are stacked together via weak van der Waals interactions [54]. As one of the typically-layered 2D TMD semiconductors from group IVB, zirconium diselenide (ZrSe_2) has garnered special interest from researchers recently. In 2017, the unique layer number dependence of the bandgap value for ZrSe_2 was demonstrated by Michal et al., where a ZrSe_2 monolayer has an indirect bandgap value of 1.2 eV, and the bandgap value of a ZrSe_2 multilayer is 0.9 eV, which facilitates the low-voltage operation of nanoscale transistors [55]. Zhang et al. studied the room temperature mobility of 14 different 2D semiconductors, and proved that ZrSe_2 had a remarkably high photon-limited mobility of above $2300 \text{ cm}^2 \text{ Vs}^{-1}$ at room temperature, which will be one of the important factors for the future development of high-performance nanoelectronics and optoelectronics [48,56]. In 2018, based on the first-principles calculation within the framework of density functional theory, Zhao et al. modulated the electronic and magnetic properties of single layer ZrSe_2 by doping. Their finding suggested that ZrSe_2 is a promising candidate for promoting progress in spintronic devices [50]. Furthermore, Jiang indicated that ZrSe_2 can be considered to be a potential candidate for third-generation solar cells owing to its bandgaps within the range of the visible and infrared [53]. Additionally, the thermoelectronic properties and electrochemical characteristics of ZrSe_2 have also been investigated by some researchers, who found that single layer ZrSe_2 has more excellent thermoelectronic properties than that of MoS_2 and MoSe_2 (the 2D semiconducting TMDs from group VIB) [50,51,57]. However, to the best of our knowledge, no previous studies have investigated the nonlinear absorption properties of ZrSe_2 in ultra-fast lasers. Owing to its comparable properties with previously reported TMDs, ZrSe_2 is expected to exhibit equally excellent saturable absorption properties.

In this work, a ZrSe_2 -polyvinyl alcohol (PVA) film was successfully prepared, which was employed as a SA to demonstrate a passively mode-locking erbium (Er)-doped fiber laser for the first time. Additionally, the appearance and nonlinear optical absorption characteristics of the prepared ZrSe_2 -PVA film were also investigated, and the saturation intensity and modulation depth were 12.72 MW/cm^2 and 2.3%, respectively. A stable soliton state with a maximum output power of 11.37 mW and a narrowest monopulse duration of 12.5 ps at a repetition frequency of 21.22 MHz was detected. Our experimental results proved that, compared with the reported TMDs before, ZrSe_2 has parallel

optical absorption characteristics and equally excellent performance, which shows that ZrSe₂ can extensively promote the development of ultrafast pulse fiber lasers.

2. Preparation and Characterization of ZrSe₂-Based SAs

2.1. Preparation Process of ZrSe₂ SAs

Figure 1 displays the process of preparing the ZrSe₂-PVA film-type SA. As is shown in the figure, a common method called liquid-phase exfoliation was applied in our experiment for preparing the ZrSe₂ dispersion solution, as well as the ZrSe₂-PVA dispersion solution, while the formation of the ZrSe₂-PVA film-type SA utilized the spin coating method. For a start, 0.1 g ZrSe₂ nanocrystals (NCs) were mixed with 30 mL 30% alcohol. The mixture was placed in a high-power ultrasonic cleaner for 8 h and then centrifuged at a speed of 2000 rpm for 30 minutes in order to prepare the ZrSe₂ homogeneous mixture. Hence, the ZrSe₂ solution was acquired. Next, a 5 wt.% PVA solution was added into the ZrSe₂ homogeneous mixture at a volume ratio of 1:1. The homogeneous ZrSe₂-PVA dispersion solution was obtained after placing the mixture in the working ultrasonic cleaner for 4 h. In our work, PVA was selected as a matrix instead of other commercially-available materials due to its excellent properties of long time stability, low cost, high damage threshold, easy film formation, and so on. After that, in order to obtain a thin film, 150 μ L ZrSe₂-PVA homogeneous mixture was spin coated onto a culture dish and dried in the drying oven at 30 °C for 24 h. Finally, a 1 \times 1 mm² square was stripped from the thin film and placed between the two facets of the fiber jumper and connected with a connector for making SAs. In this way, the ZrSe₂-PVA film-type SA could be prepared successfully.

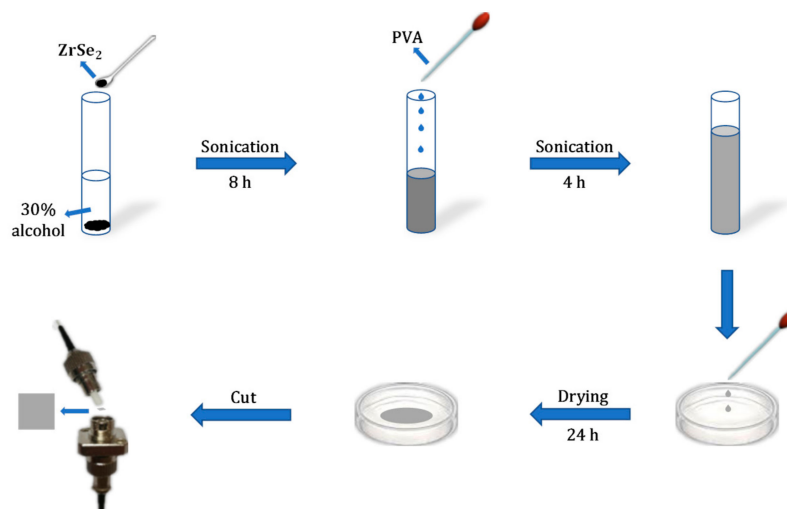


Figure 1. The preparation process of the ZrSe₂-PVA film-type SA.

2.2. Characterization Results of ZrSe₂ SAs

In order to investigate the characteristics of the ZrSe₂ NCs, we used a scanning electron microscopy (SEM, Sigma 500, ZEISS, Zeiss, Jena, Germany), an energy dispersive spectrometer (EDS, QUANTAX EDS, Bruker, Karlsruhe, Germany) and a Raman spectrometer (Horiba HR Evolution, Kyoto, Japan). It is well known that the surface morphology characteristics of the samples used in our experiment are important for analyzing the performance of the SA. Thus, based on SEM, the SEM image of the ZrSe₂ NCs at a resolution of 1 μ m is shown in Figure 2a; moreover, the inset in Figure 2a illustrates a zoomed-in SEM image at a resolution of 200 nm. As is depicted, the used sample exhibits an obvious typical layered structure, which indicates that a monolayer or a few layers of ZrSe₂ NCs will be obtained after using liquid-phase exfoliation technology. For measuring the quantitative elemental composition of the ZrSe₂ NCs, EDS was applied for characterizing the microstructure. Figure 2b depicts the chemical composition of our sample. As is shown, the typical peaks attributed to Zr and

Se can be easily observed; meanwhile, the atomic ratio of Zr and Se is 36.15:63.85, which is close to 1:2. The structural characteristics of the ZrSe₂ NCs, which were excited by a 532 nm laser, were also investigated using Raman spectroscopy. It can be seen from Figure 2c, the Raman spectrum with two characteristic peaks was detected in the range of 125–220 cm⁻¹, where the two active modes are A_{1g} and E_g modes with photon frequencies of 193.16 and 141.20 cm⁻¹, which corresponds well with previous work [58]. These results suggest that the pure ZrSe₂ NCs were prepared successfully. In addition, in order to characterize the absorption characteristic of the ZrSe₂-PVA film, the linear transmission of the ZrSe₂-PVA film and the substrate as a function of the wavelength were investigated using a ultraviolet/visible/near infrared (UV/vis/NIR) spectrophotometer (Hitachi U-4100, Tokyo, Japan). It is obvious that the linear transmittance of the ZrSe₂-PVA film increased with the increase of the optical wavelength, as shown in Figure 2d, while the transmission was measured as 89.70% at the wavelength of 1562 nm. Furthermore, as is seen from Figure 2d, the ZrSe₂-PVA film has a broad range of absorption, which extends from visible light to near infrared (NIR) light, indicating that the ZrSe₂-PVA film can be considered as promising for the development of photonics devices in the visible or NIR region.

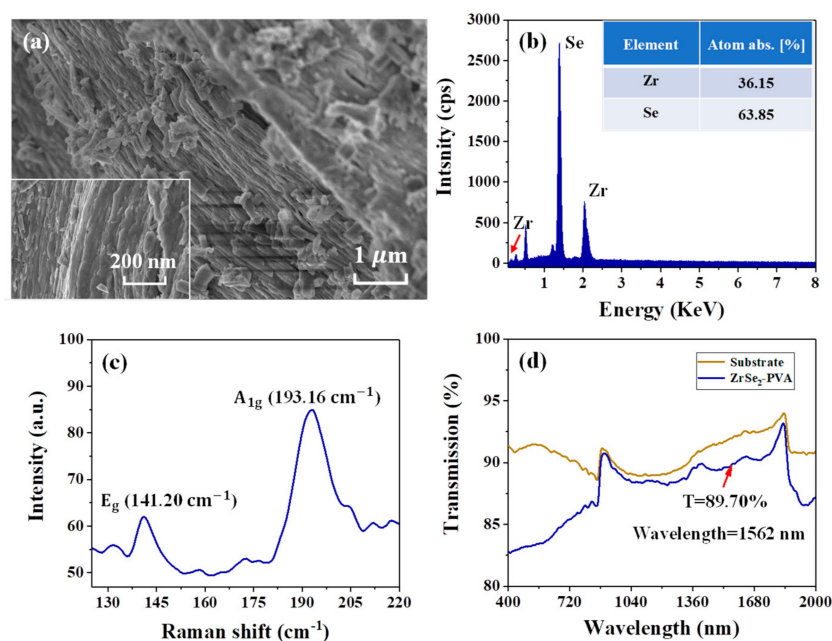


Figure 2. (a) Scanning electron microscopy (SEM) image of the ZrSe₂ nanocrystals (NCs) at a resolution of 1 μm. Inset shows the SEM image at a resolution of 200 nm. (b) Energy dispersive spectrometer (EDS) spectrum of the ZrSe₂ NCs. (c) Raman spectrum of the ZrSe₂ power. (d) Linear transmission curve of the ZrSe₂-PVA film and the substrate as a function of the wavelength.

Additionally, the nonlinear saturable absorption characteristics of the ZrSe₂-PVA film were also studied by using transmission technology related to power. A home-manufactured nonlinear polarization rotating Er-doped mode-locking fiber laser with a pulse duration of 560 fs under a center wavelength of 1580 nm, as well as a repetition frequency of 33.6 MHz, was used as the pump source. The experimental results, which were recorded by two power meters, can be seen in Figure 3. Furthermore, the following conventional equation can be employed for fitting the obtained experimental data [59]:

$$T(I) = 1 - \Delta T \times \exp(-I/I_{sat}) - T_{ns} \quad (1)$$

where $T(I)$ is the transmission rate, I is the input intensity of the laser, ΔT represents the modulation depth, I_{sat} is the saturation intensity, and T_{ns} is the non-saturable absorbance. Figure 3 also depicts the fitting curve of the experimental results. As is shown, the saturation intensity of the ZrSe₂-PVA film is

12.72 MW/cm², while the modulation depth is 2.3%, indicating that the prepared ZrSe₂-PVA film can be used as an excellent SA.

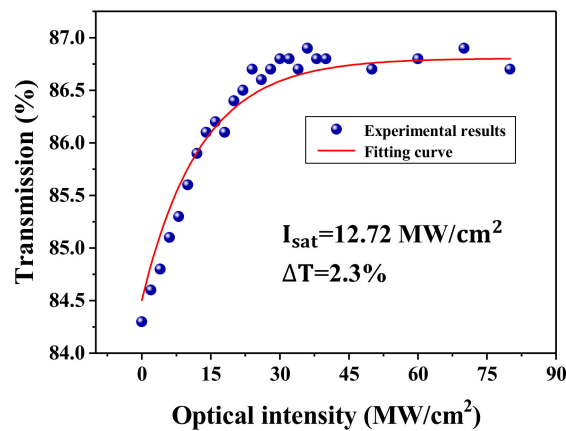


Figure 3. The nonlinear absorption characteristics of the ZrSe₂-PVA film.

3. Experimental Setup

Figure 4 shows a schematic diagram of our experiment. In our work, the pump source, which was a 976 nm laser diode (LD), was employed for generating a 980 nm laser. A ring cavity laser, including a wavelength division multiplexer (WDM) (980/1550), a Er-doped fiber (Er-80,8/125), a polarization-independent isolator (PI-ISO), a ZrSe₂-PVA film-type SA, two polarization controllers (PCs), and a 90:10 output coupler (OC), was employed for investigating the performance of the ZrSe₂-PVA film. The Er-doped fiber served as the laser gain medium, which had a length of 37 cm and a dispersion parameter of approximately 15.4 ps/(nm·km), while the dispersion parameter of the single-mode fiber used in this study was about 17.7 ps/(nm·km). The PCs were employed for changing the polarization state, and the PI-ISO was used for ensuring unidirectional delivery of light through the cavity. The ZrSe₂-PVA film-type SA was placed between the PI-ISO and one of the PCs. The 90% OC port was considered as one part of the ring cavity, while the 10% port was used to export the laser. Additionally, it is an indisputable fact that, in an all-anomalous-dispersion regime, the generation of various solitons is attributed to the dynamic equilibrium between the anomalous dispersion, the fiber nonlinear effects, and the total cavity gain and loss. In our experiment, the mode-locking operation was detected when the length of the total cavity reached 9.67 m by changing the state of the PCs, as well as the amplitude of the pump power. Thus, the intracavity net dispersion was calculated to be about -0.2213 ps^2 , with a cavity length of 9.67 m. Additionally, a fast-speed photodetector (3GHz), a digital oscilloscope (DPO3054), an optical spectrum analyzer (AQ6317B, Yokogawa, Tokyo, Japan), a radio-frequency (RF) spectrum analyzer (R&S FPC1000, Jena Germany) and a power meter (PM100D-S122C, Thorlabs, New Jersey, American) were employed to record the output characteristics of the fiber laser.

the mode-locked phenomenon could still be recorded, which means that the SA has a high damage threshold, which was greater than 544.1 mW. Moreover, the optical conversion efficiency was calculated to be 2.09% at the maximum output power of 11.37 mW. As described above, the output power and optical-to-optical conversion efficiency both had low values, which were also mostly attributed to the high insertion loss of the SA; the insert loss of the SA was calculated to be about 0.5 dB from the data of Figure 2d. Therefore, it was necessary for us to reduce the total insertion loss in order to obtain a low threshold and high optical conversion efficiency, and this will be investigated in one of our future studies. We detected the typical pulse train of the mode-locking operation by the photodetector combined with the digital oscilloscope, which is displayed in Figure 5c, where the top height of the mode-locking pulse train is consistent, without obvious fluctuation. As can be seen from Figure 5c, the time interval from pulse to pulse was 47.122 ns with a repetition frequency of 21.22 MHz, matching well with the round-trip time of the ring laser cavity, which indicated that the output pulses were attributed to the mode-locked operation. Thus, as depicted in Figure 5b, the single pulse energy increased from 0.32 to 0.54 nJ according to the output powers and the repetition frequency of 21.22 MHz. Figure 5d illustrates a zoomed-in monopulse sharp involved in the mode-locking pulse train with a monopulse duration of 1.022 ns. It is worth mentioning that the single pulse duration recorded here cannot reflect the real pulse width of the ultra-fast pulse because of the slow response times of the photodetector and the digital oscilloscope. Thus, based on the theory of mode-locked soliton, we assumed that the obtained laser pulse shape was the perfect Sech type. The theoretical pulse duration $\Delta\tau$ can be calculated based on the following formula, called the time-bandwidth product (TBP):

$$TBP = \Delta\tau \times \left(\frac{c}{\lambda_c^2} \times \Delta\lambda \right) \quad (2)$$

where c represents the light velocity (2.9979×10^8 m/s), λ_c is the center wavelength, and $\Delta\lambda$ is the spectrum width (full width at half maxima, FWHM). Thus, based on the above data, the calculated pulse duration $\Delta\tau$ is approximately 12.5 ps. However, due to the narrow 3 dB spectrum width, the pulse width was wider than previous works [34,35,37,39]. In our experiment, we also recorded other soliton operations; however, the solitons detected could not exhibit a stable state. Therefore, in our next work, in order to investigate more mode-locking phenomena, we will try to optimize the parameters of the SA, such as the modulation depth and saturation intensity, or change the dispersion of the resonant cavity by adjusting the length of the Er-doped and single-mode fiber.

It is well known that the stability can be considered one of the crucial factors in determining whether the mode-locking fiber laser can be used for practical applications. For testing the stability of the mode-locking fiber laser based on the ZrSe₂-PVA film-type SA, the RF spectra were measured using the RF spectrum analyzer combined with the photodetector. It can be seen from Figure 6a that the RF output spectrum of the mode-locking fiber laser was obtained, which was located at the fundamental frequency of 21.22 MHz, with a bandwidth of 22 MHz, as well as a resolution of 1 kHz. Moreover, the signal-to-noise ratio (SNR) was about 48 dB. Therefore, the results as shown in Figure 6a suggested that the mode-locking operation exhibited an excellent stability. Additionally, RF spectra with a broad band of 800 MHz were also recorded and are depicted in Figure 6b. As shown, the resolution of the RF spectra was 3 kHz, which further demonstrated that the state of the single mode-locking pulse exhibited a high stability. However, as illustrated in Figure 6b, the top of the RF spectra was not very flat, which shows that the mode-locking operation could be further improved in our work. In addition, the thermal effect of the PVA under high pump power also affects the stability of the mode-locked operation. Due to the high threshold power of the mode-locking operation as mentioned above, the ZrSe₂-PVA film suffered from thermal effects, which had an impact on the stable mode-locking state. Therefore, the RF spectra within a wide bandwidth shows a component of instability. Based on this, in our future works, we will be focusing on obtaining a more stable mode-locked operation under a lower pump power.

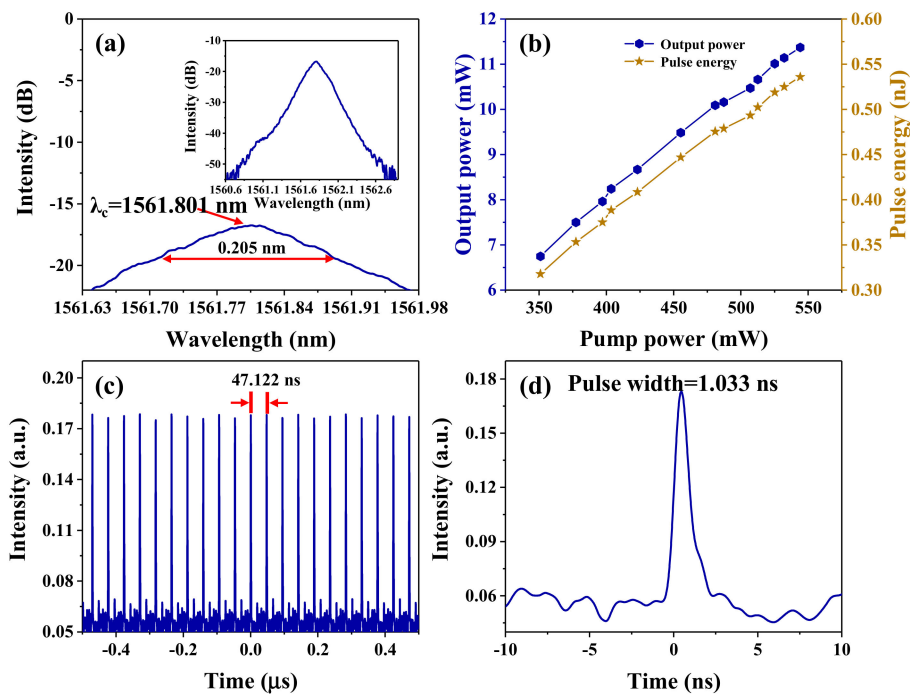


Figure 5. (a) The output optical spectrum (inset: the emission optical spectrum with a 2 nm span). (b) The output power and the single pulse energy versus the pump power. (c) The typical pulse train of the mode-locking operation. (d) The zoomed-in monopulse profile of the mode-locking operation.

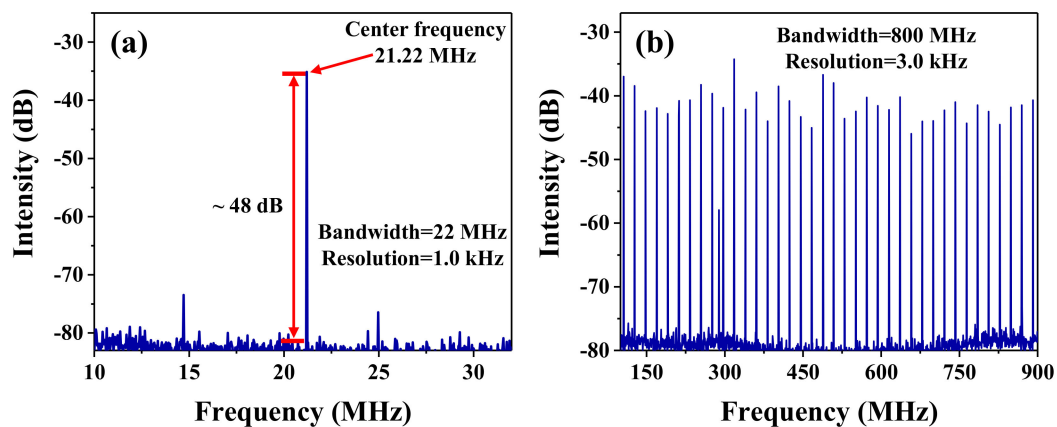


Figure 6. (a) The RF output spectrum of the mode-locking laser with the fundamental frequency of 21.22 MHz. (b) The RF spectra with a band width of a 800 MHz range.

In order to further test the performance of the fiber laser in our experiment, we studied a series of output optical spectra and 3 dB spectrum widths, as well as the theoretical duration of the single pulse at different pump powers. As shown in Figure 7a, when the PCs were fixed in a state of mode-locked operation, the emission spectra of different pump powers were recorded. It is obvious that the intensity and central wavelength of the optical spectra remain almost unchanged when the pump power increased from 351 to 544.1 mW. The corresponding 3 dB spectrum band width and the theoretical monopulse duration are depicted in Figure 7b. When the pump powers were adjusted from the threshold power to the full pump, the 3 dB bandwidth increased from 0.183 to 0.205 nm, and the variety of spectrum width was about 0.034 nm. Meanwhile, the theoretical duration of the single mode-locking pulse, which was calculated according to Equation (2), decreased from 14 to 12.5 ps as the pump powers were regulated from the threshold power to the full pump. As is shown,

the narrowest pulse width of 12.5 ps could be obtained when the pump power was set at 544.1 mW. Obviously, the monopulse duration could be further narrowed by increasing the pump power. Thus, our future work will focus on looking for enhancing the damage threshold of the ZrSe₂-PVA film-type SA in order to further narrow the monopulse duration of the passively mode-locking fiber lasers.

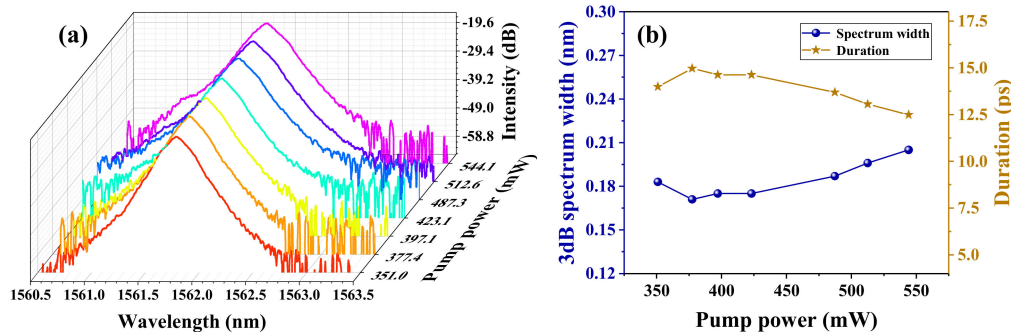


Figure 7. (a) The output optical spectrum at different pump powers. (b) The 3 dB spectrum width and the theoretical duration of the single mode-locking pulse versus the pump power.

5. Conclusions

In conclusion, ZrSe₂ was used as a SA to demonstrate a passively mode-locked Er-doped fiber laser for the first time. Moreover, the nonlinear absorption characteristics of the ZrSe₂-PVA film were investigated in our experiment, where the saturation intensity of the ZrSe₂-PVA film was 12.72 MW/cm², while the modulation depth was 2.3%. The stable passive mode-locked state with a maximum output power of 11.37 mW, under a pump power of 544.1 mW, was obtained. Meanwhile, the narrowest single pulse width was as short as 12.5 ps at a repetition frequency of 21.22 MHz. All experimental results fully verified that the ZrSe₂-PVA film-type SA had a high damage threshold and excellent nonlinear absorption characteristics, which suggested that few-layer ZrSe₂ used as an advanced material would have extensive application prospects within the field of ultra-fast pulse fiber lasers.

Author Contributions: M.W. and Y.Z. conceived and designed the experiments; L.G. and H.Z. fabricated and tested the ultra-fast modulator; M.W., H.Z. and X.C. analyzed the experimental data; M.W., H.Z. and D.L. wrote, reviewed and edited the paper.

Funding: This work was supported in part by the National Natural Science Foundation of China (Grant Nos. 61971271, 11904213, 11747149), Shandong Province Natural Science Foundation (ZR2018QF006), China Postdoctoral science Foundation (2016M602177), and supported by “Opening Foundation of Shandong Provincial Key Laboratory of Laser Technology and Application”.

Conflicts of Interest: The authors declare no conflict of interest.

References

- Sotor, J.; Sobon, G.; Abramski, L.M. Sub-130 fs mode-locked Er-doped fiber laser based on topological insulator. *Opt. Express* **2014**, *22*, 13244–13249. [[CrossRef](#)] [[PubMed](#)]
- Ming, N.; Tao, S.N.; Yang, W.Q.; Chen, Q.Y.; Sun, R.Y.; Wang, C.; Wang, S.Y.; Man, B.Y.; Zhang, H.N. Mode-locked Er-doped fiber laser based on PbS/CdS core/shell quantum dots as saturable absorber. *Opt. Express* **2018**, *26*, 9017–9026. [[CrossRef](#)] [[PubMed](#)]
- Xu, C.; Wise, F.W. Recent advances in fibre lasers for nonlinear microscopy. *Nat. Photonics* **2013**, *7*, 875–882. [[CrossRef](#)] [[PubMed](#)]
- Yan, P.; Liu, A.; Chen, Y.; Chen, H.; Ruan, S.; Guo, C.; Chen, S.; Li, I.L.; Yang, H.; Hu, J.; et al. Microfiber-based WS₂-film saturable absorber for ultra-fast photonics. *Opt. Mater. Express* **2015**, *5*, 479–489. [[CrossRef](#)]
- Keller, U. Recent developments in compact ultrafast lasers. *Nature* **2003**, *424*, 831–838. [[CrossRef](#)] [[PubMed](#)]
- Zhang, H.N.; Liu, J. Gold nanopyramids as saturable absorbers for passively Q-switched laser generation in the 1.1 μm region. *Opt. Lett.* **2016**, *41*, 1150–1152. [[CrossRef](#)]

7. Fermann, M.E.; Hartl, I. Ultrafast fibre lasers. *Nat. Photonics* **2013**, *7*, 868–874. [[CrossRef](#)]
8. Guo, B. 2D noncarbon materials-based nonlinear optical devices for ultrafast photonics. *Chin. Opt. Lett.* **2018**, *16*, 020004. [[CrossRef](#)]
9. Yang, W.; Xu, N.; Zhang, H. Nonlinear absorption properties of indium selenide and its application for demonstrating pulsed Er-doped fiber laser. *Laser Phys. Lett.* **2018**, *15*, 105101. [[CrossRef](#)]
10. Guo, Q.; Pan, J.; Li, D.; Shen, Y.; Han, X.; Gao, J.; Man, B.; Zhang, H.; Jiang, S. Versatile mode-locked operations in an Er-doped fiber laser with a film-type indium tin oxide saturable absorber. *Nanomaterials* **2019**, *9*, 701. [[CrossRef](#)]
11. Guo, L.; Shang, X.; Zhao, R.; Zhang, H.; Li, D. Nonlinear optical properties of ferromagnetic insulator Cr₂Ge₂Te₆ and its application for demonstrating pulsed fiber laser. *Appl. Phys. Express* **2019**, *12*, 082006. [[CrossRef](#)]
12. Guo, Q.; Pan, J.; Liu, Y.; Si, H.; Lu, Z.; Han, X.; Gao, J.; Zuo, Z.; Zhang, H.; Jiang, S. Output energy enhancement in a mode-locked Er-doped fiber laser using CVD-Bi₂Se₃ as a saturable absorber. *Opt. Express* **2019**, *27*, 24670–24681. [[CrossRef](#)]
13. Geim, A.K.; Novoselov, K.S. The rise of graphene. *Nat. Mater.* **2007**, *6*, 183–191. [[CrossRef](#)] [[PubMed](#)]
14. Bao, Q.; Zhang, H.; Wang, Y.; Ni, Z.; Yan, Y.; Shen, Z.; Loh, K.P.; Tang, D. Atomic-layer graphene as a saturable absorber for ultrafast pulsed lasers. *Adv. Funct. Mater.* **2009**, *19*, 3077–3083. [[CrossRef](#)]
15. Zhang, H.; Tang, D.; Zhao, L.; Bao, Q.; Loh, K.P. Large energy mode locking of an erbium-doped fiber laser with atomic layer graphene. *Opt. Express* **2009**, *17*, 17630–17635. [[CrossRef](#)] [[PubMed](#)]
16. Zhang, H.; Tang, D.; Knize, R.J.; Zhao, L.; Bao, Q.; Loh, K.P. Graphene mode locked, wavelength-tunable, dissipative soliton fiber laser. *Appl. Phys. Lett.* **2010**, *96*, 111112. [[CrossRef](#)]
17. Zhang, H.; Tang, D.; Zhao, L.; Bao, Q.; Loh, K.P.; Lin, B.; Tjin, S.C. Compact graphene mode-locked wavelength-tunable erbium-doped fiber lasers: From all anomalous dispersion to all normal dispersion. *Laser Phys. Lett.* **2010**, *7*, 591–596. [[CrossRef](#)]
18. Popa, D.; Sun, Z.; Torrisi, F.; Hasan, T.; Wang, F.; Ferrari, A.C. Sub 200 fs pulse generation from a graphene mode-locked fiber laser. *Appl. Phys. Lett.* **2010**, *97*, 203106. [[CrossRef](#)]
19. Sun, Z.; Hasan, T.; Torrisi, F.; Popa, D.; Privitera, G.; Wang, F.; Bonaccorso, F.; Basko, D.M.; Ferrari, A.C. Graphene mode-locked ultrafast laser. *ACS Nano* **2010**, *4*, 803–810. [[CrossRef](#)]
20. Sun, Z.; Popa, D.; Hasan, T.; Torrisi, F.; Wang, F.; Kelleher, E.J.R.; Travers, J.C.; Nicolosi, V.; Ferrari, A.C. A stable, wideband tunable, near transform-limited, graphene-mode-locked, ultrafast laser. *Nano Res.* **2010**, *3*, 653–660. [[CrossRef](#)]
21. Bonaccorso, F.; Sun, Z.; Hasan, T.; Ferrari, A.C. Graphene photonics and optoelectronics. *Nat. Photonics* **2010**, *4*, 611–622. [[CrossRef](#)]
22. Wang, Z.T.; Chen, Y.; Zhao, C.J.; Zhang, H.; Wen, S.C. Switchable dual-wavelength synchronously Q-switched erbium-doped fiber laser based on graphene saturable absorber. *IEEE Photonics J.* **2012**, *4*, 869–876. [[CrossRef](#)]
23. Jung, M.; Koo, J.; Park, J.; Song, Y.; Jhon, Y.M.; Lee, K.; Lee, S.; Lee, J.H. Mode-locked pulse generation from an allfiberized, Tm-Ho-codoped fiber laser incorporating a graphene oxide-deposited sidepolished fiber. *Opt. Express* **2013**, *21*, 20062–20072. [[CrossRef](#)] [[PubMed](#)]
24. Tolstik, N.; Sorokin, E.; Sorokina, I.T. Graphene mode-locked Cr:ZnS laser with 41 fs pulse duration. *Opt. Express* **2014**, *22*, 5564–5571. [[CrossRef](#)]
25. Luo, A.P.; Zhu, P.F.; Liu, H.; Zheng, X.W.; Zhao, N.; Liu, M.; Cui, H.; Luo, Z.C.; Xu, W.C. Microfiber-based, highly nonlinear graphene saturable absorber for formation of versatile structural soliton molecules in a fiber laser. *Opt. Express* **2014**, *22*, 27019–27025. [[CrossRef](#)] [[PubMed](#)]
26. Huang, S.; Wang, Y.; Yan, P.; Zhao, J.; Li, H.; Lin, R. Tunable and switchable multi-wavelength dissipative soliton generation in a graphene oxide mode-locked Yb-doped fiber laser. *Opt. Express* **2014**, *22*, 11417–11426. [[CrossRef](#)] [[PubMed](#)]
27. Wan, H.; Cai, W.; Wang, F.; Jiang, S.; Xu, S.; Liu, J. High-quality monolayer graphene for bulk laser mode-locking near 2 μm. *Opt. Quant. Electron.* **2015**, *48*, 1–8. [[CrossRef](#)]
28. Martinez, A.; Sun, Z. Nanotube and graphene saturable absorbers for fibre lasers. *Nat. Photonics* **2013**, *7*, 842–845. [[CrossRef](#)]
29. Hsieh, D.; Qian, D.; Wray, L.; Xia, Y.; Hor, Y.S.; Cava, R.J.; Hasan, M.Z. A topological Dirac insulator in a quantum spin Hall phase. *Nature* **2008**, *452*, 970–974. [[CrossRef](#)]

30. Zhang, H.; Liu, C.X.; Qi, X.L.; Dai, X.; Fang, Z.; Zhang, S.C. Topological insulators in Bi₂Se₃, Bi₂Te₃ and Sb₂Te₃ with a single Dirac cone on the surface. *Nat. Phys.* **2009**, *5*, 438–442. [[CrossRef](#)]
31. Luo, Z.C.; Liu, M.; Liu, H.; Zheng, X.W.; Luo, A.P.; Zhao, C.J.; Zhang, H.; Wen, S.C.; Xu, W.C. 2 GHz passively harmonic mode-locked fiber laser by a microfiber-based topological insulator saturable absorber. *Opt. Lett.* **2013**, *38*, 5212–5215. [[CrossRef](#)] [[PubMed](#)]
32. Liu, H.; Zheng, X.W.; Liu, M.; Zhao, N.; Luo, A.P.; Luo, Z.C.; Xu, W.C.; Zhang, H.; Zhao, C.J.; Wen, S.C. Femtosecond pulse generation from a Topological Insulator mode-locked fiber laser. *Opt. Express* **2014**, *22*, 6868–6873. [[CrossRef](#)]
33. Xu, N.N.; Ming, N.; Han, X.L.; Man, B.Y.; Zhang, H. Large-energy passively Q-switched Er-doped fiber laser based on CVD-Bi₂Se₃ as saturable absorber. *Opt. Mater. Express* **2019**, *9*, 373–383. [[CrossRef](#)]
34. Lin, Y.S.; Yang, C.Y.; Lin, S.F.; Tseng, W.H.; Bao, Q.; Wu, C.I.; Lin, G.R. Soliton compression of the erbium-doped fiber laser weakly started mode-locking by nanoscale p-type Bi₂Te₃ topological insulator particles. *Laser Phys. Lett.* **2014**, *11*, 055107. [[CrossRef](#)]
35. Sotor, J.; Sobon, G.; Macherzynski, W.; Abramski, K.M. Harmonically mode-locked Er-doped fiber laser based on a Sb₂Te₃ topological insulator saturable absorber. *Laser Phys. Lett.* **2014**, *11*, 055102. [[CrossRef](#)]
36. Xu, H.; Wan, X.; Ruan, Q.; Yang, R.; Du, T.; Chen, N.; Cai, Z.; Luo, Z. Effects of nanomaterial saturable absorption on passively mode-locked fiber lasers in anomalous dispersion regime: Simulations and experiments. *IEEE J. Sel. Top. Quant.* **2018**, *24*, 1100209. [[CrossRef](#)]
37. Wang, K.; Wang, J.; Fan, J.; Lotya, M.; Neill, A.O.; Fox, D.; Feng, Y.; Zhang, X.; Jiang, B.; Zhao, Q.; et al. Ultrafast Saturable Absorption of Two-Dimensional MoS₂ Nanosheets. *ACS Nano* **2013**, *7*, 9260–9267. [[CrossRef](#)]
38. Hu, Q.Y.; Zhang, X.Y.; Liu, Z.J.; Li, P.; Li, M.; Cong, Z.H.; Qin, Z.G.; Chen, X.H. High-order harmonic mode-locked Yb-doped fiber laser based on a SnSe₂ saturable absorber. *Opt. Laser Technol.* **2019**, *119*, 105639. [[CrossRef](#)]
39. Mao, D.; She, X.; Du, B.; Yang, D.; Zhang, W.; Song, K.; Cui, X.; Jiang, B.; Peng, T.; Zhao, J. Erbium-doped fiber laser passively mode locked with few-layer WSe₂/MoSe₂ nanosheets. *Sci. Rep.* **2016**, *6*, 23583. [[CrossRef](#)]
40. Li, J.; Zhao, Y.; Chen, Q.; Niu, K.; Sun, R.; Zhang, H. Passively mode-locked ytterbium-doped fiber laser based on SnS₂ as saturable absorber. *IEEE Photonics J.* **2017**, *9*, 1506707. [[CrossRef](#)]
41. Mao, D.; Cui, X.; Gan, X.; Li, M.; Zhang, W.; Lu, H.; Zhao, J. Passively Q-switched and mode-locked fiber laser based on a ReS₂ saturable absorber. *IEEE J. Sel. Top. Quant.* **2018**, *24*, 1100406. [[CrossRef](#)]
42. Chen, Y.; Jiang, G.; Chen, S.; Guo, Z.; Yu, X.; Zhao, C.; Zhang, H.; Bao, Q.; Wen, S.; Tang, D.; et al. Mechanically exfoliated black phosphorus as a new saturable absorber for both Q-switching and mode-locking laser operation. *Opt. Express* **2015**, *23*, 12823–12833. [[CrossRef](#)] [[PubMed](#)]
43. Sotor, J.; Sobon, G.; Kowalczyk, M.; Macherzynski, W.; Paletko, P.; Abramski, K.M. Ultrafast thulium-doped fiber laser mode locked with black phosphorus. *Opt. Lett.* **2015**, *40*, 3885–3888. [[CrossRef](#)] [[PubMed](#)]
44. Luo, Z.C.; Liu, M.; Guo, Z.N.; Jiang, X.F.; Luo, A.P.; Zhao, C.J.; Yu, X.F.; Xu, W.C.; Zhang, H. Microfiber-based few-layer black phosphorus saturable absorber for ultra-fast fiber laser. *Opt. Express* **2015**, *23*, 20030–20039. [[CrossRef](#)] [[PubMed](#)]
45. Ma, J.; Lu, S.; Guo, Z.; Xu, X.; Zhang, H.; Tang, D.; Fan, D. Few-layer black phosphorus based saturable absorber mirror for pulsed solid-state lasers. *Opt. Express* **2015**, *23*, 22643–22648. [[CrossRef](#)] [[PubMed](#)]
46. Xu, Y.; Wang, Z.; Guo, Z.; Huang, H.; Xiao, Q.; Zhang, H.; Yu, X.F. Solvothermal synthesis and ultrafast photonics of black phosphorus quantum dots. *Adv. Opt. Mater.* **2016**, *4*, 1223–1229. [[CrossRef](#)]
47. Jin, X.; Hu, G.; Zhang, M.; Hu, Y.; Owen, T.A.; Howe, R.C.T.; Wu, T.C.; Wu, Q.; Zheng, Z.; Hasan, T. 102 fs pulse generation from a long-term stable, inkjet-printed black phosphorus-mode-locked fiber laser. *Opt. Express* **2018**, *26*, 12506–12513. [[CrossRef](#)]
48. Jaiswal, H.N.; Liu, M.; Shahi, S.; Yao, F.; Zhao, Q.; Xu, X.; Li, H. Localized surface plasmon resonance on two-dimensional HfSe₂ and ZrSe₂. *Semicond. Sci. Technol.* **2018**, *33*, 124014. [[CrossRef](#)]
49. Muhammad, Z.; Mu, K.; Lv, H.; Wu, C.; Rehman, Z.U.; Habib, M.; Sun, Z.; Wu, X.; Song, L. Electron doping induced semiconductor to metal transitions in ZrSe₂ layers via copper atomic intercalation. *Nano Res.* **2018**, *11*, 4914–4922. [[CrossRef](#)]
50. Zhao, X.; Zhang, H.; Chen, T.; Gao, Y.; Wang, H.; Wang, T.; Wei, S. Modulating electronic and magnetic properties of monolayer ZrSe₂ by doping. *Superlattice. Microst.* **2018**, *120*, 659–669. [[CrossRef](#)]

51. Ōnuki, Y.; Inada, R.; Tanuma, S.; Yamanaka, S.; Kamimura, H. Electrochemical characteristics of TiS₂, ZrSe₂ and VSe₂ in secondary lithium battery. *Jpn. J. Appl. Phys.* **1981**, *20*, 1583–1588. [[CrossRef](#)]
52. Hankare, P.P.; Asabe, M.R.; Kokate, A.V.; Delekar, S.D.; Sathe, D.J.; Mulla, I.S.; Chougule, B.K. Effect of annealing on properties of ZrSe₂ thin films. *J. Cryst. Growth* **2006**, *294*, 254–259. [[CrossRef](#)]
53. Jiang, H. Structural and electronic properties of ZrX₂ and HfX₂ (X = S and Se) from first principles calculations. *J. Chem. Phys.* **2011**, *134*, 204705. [[CrossRef](#)] [[PubMed](#)]
54. Valero, S.M.; López, V.G.; Cantarero, A.; Galbiati, M. Raman spectra of ZrS₂ and ZrSe₂ from bulk to atomically thin layers. *Appl. Sci.* **2016**, *6*, 264. [[CrossRef](#)]
55. Mleczo, M.J.; Zhang, C.; Lee, H.R.; Kuo, H.H.; Köpe, B.M.; Moore, R.G.; Shen, Z.X.; Fisher, I.R.; Nishi, Y.; Pop, E. HfSe₂ and ZrSe₂: Two-dimensional semiconductors with native high- κ oxides. *Sci. Adv.* **2017**, *3*, e1700481. [[CrossRef](#)]
56. Zhang, W.; Huang, Z.; Zhang, W.; Li, Y. Two-dimensional semiconductors with possible high room temperature mobility. *Nano Res.* **2014**, *7*, 1731–1737. [[CrossRef](#)]
57. Ding, G.; Gao, G.Y.; Huang, Z.; Zhang, W.; Yao, K. Thermoelectric properties of monolayer MSe₂ (M = Zr, Hf): Low lattice thermal conductivity and a promising figure of merit. *Nanotechnology* **2016**, *27*, 375703. [[CrossRef](#)]
58. Grimme, S.; Antony, J.; Ehrlich, S.; Krieg, H. A consistent and accurate ab initio parametrization of density functional dispersion correction (DFT-D) for the 94 elements H-Pu. *J. Chem. Phys.* **2010**, *132*, 154104. [[CrossRef](#)]
59. Yükek, M.; Kürüm, U.; Yaglioglu, H.G.; Elmali, A.; Ateş, A. Nonlinear and saturable absorption characteristics of amorphous InSe thin films. *J. Appl. Phys.* **2010**, *107*, 033115. [[CrossRef](#)]
60. Heebner, J.E.; Wong, V.; Schweinsberg, A.; Boyd, R.W.; Jackson, D.J. Optical transmission characteristics of fiber ring resonators. *IEEE J. Quantum Electron.* **2004**, *40*, 726–730. [[CrossRef](#)]
61. Haye, P.D.; Schliesser, A.; Arcizet, O.; Wilken, T.; Holzwarth, R.; Kippenberg, T. Optical frequency comb generation from a monolithic microresonator. *Nature* **2007**, *450*, 1214–1217.
62. Mao, D.; Jiang, B.; Zhang, W.; Zhao, J. Pulse-state switchable fiber laser mode-locked by carbon nanotubes. *IEEE Photon. Technol. Lett.* **2015**, *27*, 253–256. [[CrossRef](#)]
63. Mao, D.; Zhang, S.; Wang, Y.; Gan, X.; Zhang, W.; Mei, T.; Wang, Y.; Wang, Y.; Zeng, H.; Zhao, J. WS₂ saturable absorber for dissipative soliton mode locking at 1.06 and 1.55 μm . *Opt. Express* **2015**, *23*, 27509–27519. [[CrossRef](#)] [[PubMed](#)]
64. Guo, B.; Yu, Q.L.; Yao, Y.; Wang, P. Direct generation of dip-type sidebands from WS₂ mode-locked fiber laser. *Opt. Mater. Express* **2016**, *6*, 2475–2486. [[CrossRef](#)]
65. Wang, S.; Yu, H.; Zhang, H.; Wang, A.; Zhao, M.; Chen, Y.; Mei, L.; Wang, J. Broadband few-layer MoS₂ saturable absorbers. *J. Adv. Mater.* **2014**, *26*, 3538–3544. [[CrossRef](#)]
66. Xu, N.; Yang, W.; Zhang, H. Nonlinear saturable absorption properties of indium selenide and its application for demonstrating a Yb-doped mode-locked fiber laser. *Opt. Mater. Express* **2018**, *8*, 3092. [[CrossRef](#)]
67. Niu, K.; Sun, R.; Chen, Q.; Man, B.; Zhang, H. Passively mode-locked Er-doped fiber laser based on SnS₂ nanosheets as a saturable absorber. *Photonics Res.* **2018**, *6*, 72–76. [[CrossRef](#)]
68. Niu, K.; Chen, Q.; Sun, R.; Man, B.; Zhang, H. Passively Q-switched erbium-doped fiber laser based on SnS₂ saturable absorber. *Opt. Mater. Express* **2017**, *7*, 3934–3943. [[CrossRef](#)]
69. Peng, J.; Zhan, L.; Gu, G.; Qian, K.; Luo, S.; Shen, Q. Direct generation of 128-fs Gaussian pulses from a compensation-free fiber laser using dual mode-locking mechanisms. *Opt. Commun.* **2012**, *285*, 731–733. [[CrossRef](#)]
70. Noske, D.U.; Pandit, N.; Taylor, J.R. Source of spectral and temporal instability in soliton fiber lasers. *Opt. Lett.* **1992**, *17*, 1515–1517. [[CrossRef](#)]
71. Smith, N.J.; Blow, K.J.; Andonovic, I. Sideband generation through perturbations to the average soliton model. *J. Lightw. Technol.* **1992**, *10*, 1329–1333. [[CrossRef](#)]
72. Kelly, S.M.J. Characteristic sideband instability of periodically amplified average soliton. *Electron. Lett.* **1992**, *28*, 806–807. [[CrossRef](#)]

